AGU PUBLICATIONS

Water Resources Research

RESEARCH ARTICLE

10.1002/2015WR018204

Evaluating geothermal and hydrogeologic controls on regional groundwater temperature distribution

Erick R. Burns[1], Steven E. Ingebritsen[2], Michael Manga[3], and Colin F. Williams[4]

[1]USGS Oregon Water Science Center, Portland, Oregon, USA, [2]USGS National Research Program, Menlo Park, California, USA, [3]Department of Earth and Planetary Science, University of California—Berkeley, Berkeley, California, USA, [4]USGS Geology, Minerals, Energy, and Geophysics Science Center, Menlo Park, California, USA

Key Points:
- An analytic solution is developed to simulate combined groundwater and geothermal heat flow
- The general anisotropic form of viscous heat generation is derived for use in numerical solvers
- The Peclet Number can be used to predict the persistence of thermal plumes

Supporting Information:
- Supporting Information S1
- Supporting Information S2

Correspondence to:
E. R. Burns,
eburns@usgs.gov

Citation:
Burns, E. R., S. E. Ingebritsen, M. Manga, and C. F. Williams (2016), Evaluating geothermal and hydrogeologic controls on regional groundwater temperature distribution, *Water Resour. Res.*, *52*, doi:10.1002/2015WR018204.

Received 8 OCT 2015
Accepted 24 JAN 2016
Accepted article online 28 JAN 2016

Abstract A one-dimensional (1-D) analytic solution is developed for heat transport through an aquifer system where the vertical temperature profile in the aquifer is nearly uniform. The general anisotropic form of the viscous heat generation term is developed for use in groundwater flow simulations. The 1-D solution is extended to more complex geometries by solving the equation for piece-wise linear or uniform properties and boundary conditions. A moderately complex example, the Eastern Snake River Plain (ESRP), is analyzed to demonstrate the use of the analytic solution for identifying important physical processes. For example, it is shown that viscous heating is variably important and that heat conduction to the land surface is a primary control on the distribution of aquifer and spring temperatures. Use of published values for all aquifer and thermal properties results in a reasonable match between simulated and measured groundwater temperatures over most of the 300 km length of the ESRP, except for geothermal heat flow into the base of the aquifer within 20 km of the Yellowstone hotspot. Previous basal heat flow measurements ($\sim$110 mW/m^2) made beneath the ESRP aquifer were collected at distances of $>$50 km from the Yellowstone Plateau, but a higher basal heat flow of 150 mW/m^2 is required to match groundwater temperatures near the Plateau. The ESRP example demonstrates how the new tool can be used during preliminary analysis of a groundwater system, allowing efficient identification of the important physical processes that must be represented during more-complex 2-D and 3-D simulations of combined groundwater and heat flow.

1. Introduction

Temperature can be used as a tracer to understand hydrogeologic and geothermal processes [cf., *Smith and Chapman*, 1983; *Forster and Smith*, 1988a, 1988b, 1989; *Manga*, 2001; *Anderson*, 2005; *Saar*, 2011]. Groundwater gains or loses heat by conduction and due to chemical reactions (including radiogenic decay of isotopes in minerals), and gains heat from friction as mechanical energy is viscously dissipated along the groundwater flow path.

Manga and Kirchner [2004] demonstrated the possible importance of viscous heating in their interpretation of spring temperatures in the Cascade Range of the northwestern United States. In the Cascade Range, most hydrothermal heat discharge occurs through "slightly thermal" springs—springs with temperatures elevated less than a few degrees above local ambient [*Ingebritsen and Mariner*, 2010]. The analysis by *Manga and Kirchner* [2004] showed that the contribution of geothermal heat to such springs could be greatly overestimated—by as much as a factor of two or more—if the conversion of gravitational potential energy to heat ($\sim$2.3°C/km elevation) is not accounted for. Because of the copious groundwater recharge through young volcanic rocks of the Cascades, *Manga and Kirchner* [2004] were able to simplify their analysis by assuming near-zero heat conduction to the land surface [*Ingebritsen et al.*, 1989].

Here we consider the combined effects of the various heating mechanisms and groundwater flow in a more complex analysis, where heat conduction to the land surface is included and boundary conditions change piecewise along a flow path. We generalize the viscous heat generation term of *Manga and Kirchner* [2004], allowing application to anisotropic porous media of arbitrary geometry. An analytic solution of a simplified one-dimensional (1-D) form of the heat and groundwater flow equations is developed, and dimensional analysis of the analytic solution is used to identify the dominant physical processes. The 1-D solution is applied piece-wise to the Eastern Snake River Plain (ESRP) regional aquifer to demonstrate the method.

Geothermal heat flow through the ESRP is significantly perturbed by flow through the regional aquifer system [*Brott et al*., 1976, 1981] but, unlike the examples considered by *Manga and Kirchner* [2004], heat conduction to the land surface is a significant part of the heat flow budget. We do not assert that the 1-D solution is sufficient to capture all of the complex 3-D interactions between groundwater and heat flow within the ESRP, but we do demonstrate that the method can efficiently identify the important physical processes within the ESRP aquifer, giving the practitioner a powerful tool to make estimates, assess which parameters are most sensitive (allowing improved experimental design), and help select more complex 2-D and 3-D tools for subsequent analyses. Piece-wise application of the analytic solution is performed using an open-source Python script that is included in supporting information.

2. Derivation of the General Form of the Viscous Heat Production Term for Flow in Porous Media

Steady state conservation of mass can be written:

$$\nabla \cdot \boldsymbol{q}_m = 0 \tag{1}$$

where the mass flux (mass per area per time) is:

$$\boldsymbol{q}_m = \rho_w \boldsymbol{q} \tag{2}$$

with $\boldsymbol{q}$ being the Darcy flux and ρ_w the density of water.

Assuming no sources or sinks of heat except viscous heating, the steady state heat equation is:

$$-\nabla \cdot [e_m \boldsymbol{q}_m] + \nabla \cdot [\boldsymbol{D}^* \nabla T] + \dot{Q}_H = 0 \tag{3}$$

where is T temperature, e_m is the thermal energy per mass, $\boldsymbol{D}^*$ is a diffusion/dispersion term which in general is a tensor, and $\dot{Q}_H$ is the viscous heat production term that will be defined. The upper and lower case "*q*" is generally used in this manuscript to represent fluxes and the subscript H is used to distinguish heat flux from mass or volumetric fluid flux.

To convert the equation into thermodynamic potentials that can be measured, we use the specific heat capacity of water (c_w):

$$e_m = c_w T \tag{4}$$

A more general notion of c_w allows this parameter to vary as a function of temperature and other thermodynamic variables:

$$c_w = \left(\frac{\partial e_m}{\partial T} \right)_{(P,T,\ldots)} \tag{5}$$

which states that the specific heat capacity is the change in thermal energy that accompanies a change in temperature for a set of fixed values of the thermodynamic variables, which may in general consist of any set of thermodynamic potentials that affect the specific heat capacity (e.g., pressure, temperature, chemical potential, etc.). The total thermal energy per unit mass is then given by the integral:

$$e_m = \int_{T_0^H}^{T} c_w dT \tag{6}$$

where T_0^H is the temperature at which thermal energy equals zero (i.e., absolute zero). Substituting into the energy equation and expanding the first term:

$$-\boldsymbol{q}_m \cdot [c_w \nabla T] - c_w T (\nabla \cdot \boldsymbol{q}_m) + \nabla \cdot [\boldsymbol{D}^* \nabla T] + \dot{Q}_H = 0 \tag{7}$$

The second term is zero due to conservation of mass (equation (1)), giving:

$$-\boldsymbol{q}_m \cdot [c_w \nabla T] + \nabla \cdot [\boldsymbol{D}^* \nabla T] + \dot{Q}_H = 0 \tag{8}$$

The first term is the advective heat flux, the second term is the conductive and dispersive heat flux, and the last term is viscous heating.

Assuming that mechanical energy is converted into heat through viscous losses, the viscous heat generation term can be written in terms of a dot product of the mass flux with the gradient in the specific mechanical energy (i.e., the mechanical energy per unit mass [*Fetter*, 1994, equations (5) and (6)]):

$$\dot{Q}_H = \boldsymbol{q}_m \cdot \left[c^* \nabla \left(\frac{P}{\rho} + \frac{\boldsymbol{v} \cdot \boldsymbol{v}}{2} + gz \right) \right] \tag{9}$$

This formulation of specific mechanical energy includes contributions from pressure, kinetic energy (the water velocity term), and gravitational potential (the gravitational constant times the elevation above some datum). Similar to specific heat capacity (c_w), c^* is the change in thermal energy per unit mass associated with a change in mechanical energy:

$$c^* = \frac{\partial e_m}{\partial \left(\frac{P}{\rho} + \frac{\boldsymbol{v} \cdot \boldsymbol{v}}{2} + gz \right)} \tag{10}$$

Assuming all mechanical energy lost is converted to heat, $c^* = -1$. The resulting steady state heat flow equation is:

$$-\boldsymbol{q}_m \cdot [c_w \nabla T] + \nabla \cdot [\boldsymbol{D}^* \nabla T] - \boldsymbol{q}_m \cdot \left[\nabla \left(\frac{P}{\rho} + \frac{\boldsymbol{v} \cdot \boldsymbol{v}}{2} + gz \right) \right] = 0 \tag{11}$$

where the viscous heat generation term applies to anisotropic media, because the mass flux and the gradient in mechanical energy need not be collinear.

Under the typical groundwater flow assumption of slow flow velocity (i.e., when Darcy's Law is valid), the kinetic term is negligible, allowing the resulting equation to be written as:

$$-\boldsymbol{q}_m \cdot [c_w \nabla T] + \nabla \cdot [\boldsymbol{D}^* \nabla T] - \boldsymbol{q}_m \cdot [g \nabla h] = 0 \tag{12}$$

where the hydraulic head (h), is given by the usual relation: $h = \frac{P}{\rho g} + z$. The assumption that all mechanical energy lost is converted to heat is typically valid for groundwater systems where Darcy's Law is valid (i.e., $c^* = -1$). However, in a system where mechanical energy is converted to other thermodynamic potentials, for example, osmotic potential (e.g., p. 8–10, 119–120, 177 of *Ingebritsen et al*. [2006]) where mechanical potential may be converted to a chemical potential, this assumption needs to be reexamined. More simply stated; if Darcy's Law requires additional terms in the flow potential, then mechanical potential may be converted to forms of energy other than heat.

3. Derivation of the 1-D Steady State Analytic Model

If a thermally well-mixed aquifer is nearly isothermal with respect to depth compared to the conductive profiles above it (the vadose zone) and below it (the basal confining unit), then a 1-D analytic solution can be developed to understand the combined effects of geothermal heat flow, conduction of heat to land surface, viscous heat generation, and advection of heat along the groundwater flow path (Figure 1). Because the solution is 1-D, all vectors reduce to scalars.

Assuming that groundwater flow is uniform and the groundwater is thermally well-mixed (i.e., the temperature profile in the aquifer is nearly isothermal), the heat per unit area (E′) is the heat energy per unit volume times the aquifer saturated thickness (b) and is given by:

$$\mathrm{E}' = [\rho_s (1-\varphi) c_s + \rho_w \varphi c_w] b T \tag{13}$$

where ρ_s is density of the solid, c_s is specific heat capacity of the solid, ρ_w is density of water, c_w is specific heat capacity of water, φ is porosity, and T is temperature of the aquifer; E′ is the heat in a unit-width "slice" of the aquifer normal to the groundwater flow path.

Heat flux into the slice (q_H^{in}) is divided into three components:

1. uniform heat flow at the base (q_H^{base});
2. distributed viscous heating; and
3. heat advected into the slice.

Heat flux out of the slice (q_H^{out}) is divided into two components:

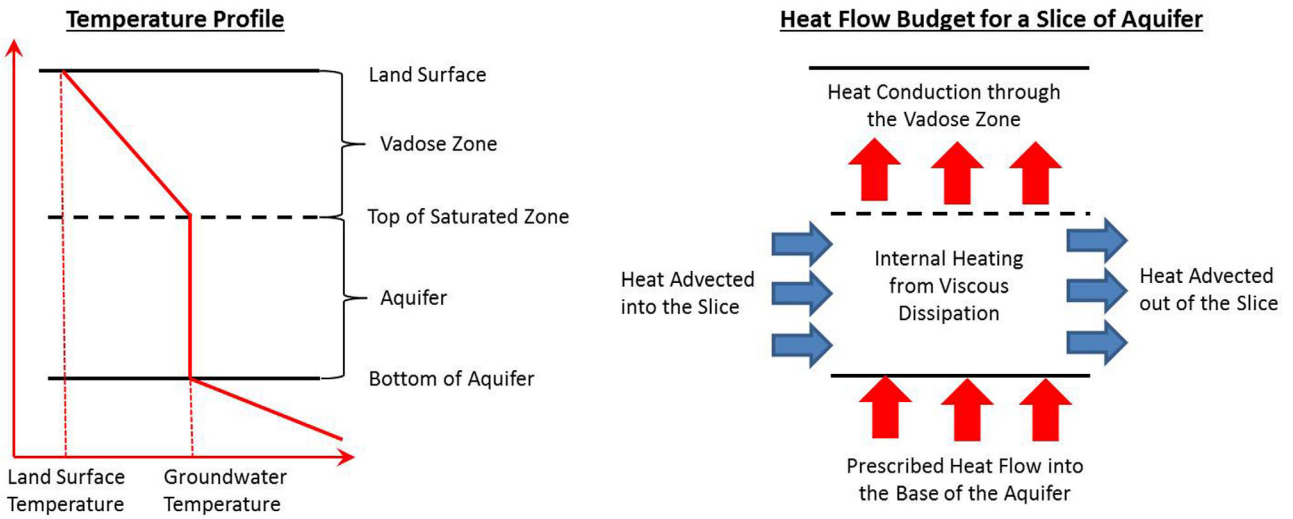

Figure 1. Diagram showing the relation between the thermal profile and the physical processes being represented by the 1-D analytic model. The differential equation is derived by considering an infinitesimally thin slice of aquifer through which groundwater flows.

1. heat conduction from the water table, assumed to the be the steady rate of heat flow controlled by vertical conduction through the vadose zone; and
2. heat advected out of the slice.

Heat conduction along the flow path (in the direction of flow) is assumed to be negligible.

Assuming steady state, conservation of energy gives:

$$\frac{dE'}{dt} = q_H^{in} - q_H^{out} = 0 \tag{14}$$

Writing an explicit form of each of the components of q_H^{in} and q_H^{out} yields:

$$0 = q_H^{base} - q_m \cdot bg\frac{dh}{ds} - \sigma_{vz}\frac{T - T_{LS}}{z_{LS} - z_{WT}} - q_m \cdot bc_w\frac{dT}{ds} \tag{15}$$

where $z_{LS} - z_{WT}$ is the depth to the water table, T_{LS} is the temperature at land surface, σ_{vz} is the bulk thermal conductivity of the vadose zone, b is the saturated thickness of the aquifer, and s is position along the groundwater flow path.

The mass flux can be written:

$$q_m = \rho_w \varphi v_w \tag{16}$$

where v_w is the scalar velocity of water along the flow path, giving:

$$0 = q_H^{base} - v_w \cdot \rho_w \varphi bg\frac{dh}{ds} - \sigma_{vz}\frac{T - T_{LS}}{z_{LS} - z_{WT}} - v_w \cdot \rho_w \varphi bc_w\frac{dT}{ds} \tag{17}$$

Because fluid flow is steady, the total volumetric flux (Q) is constant. Assuming a constant width of the aquifer system (W; the product bW is the area through which Q moves) gives the following relation:

$$v_w = \frac{q}{\varphi} = \frac{Q}{\varphi bW} \tag{18}$$

where q is the scalar Darcy flux. Because the problem is 1-D, the head and temperature gradients are in the same direction as groundwater flow, reducing all dot products to simple multiplication of scalars, giving the form of the energy conservation equation to be solved:

$$0 = q_H^{base} - \frac{Q\rho_w g}{W}\frac{dh}{ds} - \sigma_{vz}\frac{T - T_{LS}}{z_{LS} - z_{WT}} - \frac{Q\rho_w c_w}{W}\frac{dT}{ds} \tag{19}$$

In general, all terms except Q and W can be functions of s. To find analytic solutions for some cases of interest, we rewrite in the form:

$$\frac{dT}{ds} = f_0(s)T + f_1(s) + f_2(s) + f_3(s) \tag{20}$$

where:

$$f_0(s) = \frac{-W\sigma_{vz}}{Q\rho_w c_w (z_{LS} - z_{WT})} \tag{21}$$

$$f_1(s) = \frac{Wq_H^{base}}{Q\rho_w c_w} \tag{22}$$

$$f_2(s) = \frac{-g}{c_w}\frac{dh}{ds} \tag{23}$$

$$f_3(s) = -f_0(s)T_{LS} \tag{24}$$

Using the notation of *Powers* [1987, pp. 10–12], equation (20) has the solution:

$$T(s) = T_c(s) + T_{p1}(s) + T_{p2}(s) + T_{p3}(s) \tag{25}$$

where the general solution of the corresponding homogeneous equation is:

$$T_c(s) = T_0 e^{\int f_0(s)ds} \tag{26}$$

and the particular solutions for the inhomogeneities $(f_1(s), f_2(s), f_3(s))$ are, respectively:

$$T_{p1}(s) = T_c(s)\int \frac{f_1(s)}{T_c(s)}ds \tag{27}$$

$$T_{p2}(s) = T_c(s)\int \frac{f_2(s)}{T_c(s)}ds \tag{28}$$

$$T_{p3}(s) = T_c(s)\int \frac{f_3(s)}{T_c(s)}ds \tag{29}$$

and T_0 is the temperature at $s=0$ (the location where groundwater flows into the domain); the solution is valid as groundwater proceeds along the flow path ($s > 0$).

For the current case of interest, we assume that water and rock density and specific heat capacity (ρ_w, ρ_s, c_w, and c_s), saturated thickness (b), depth to the water table ($z_{LS} - z_{WT}$), basal heat flow into the aquifer (q_H^{in}), and the head gradient ($\frac{dh}{ds}$) are uniform. Further, we suppose that temperature at land surface (T_{LS}) is a linear function of s. This means that f_0, f_1, and f_2 are not functions of s, yielding:

$$T_c(s) = T_0 e^{f_0 s} \tag{30}$$

$$T_{p1}(s) = \frac{f_1}{f_0}\left(e^{f_0 s} - 1\right) \tag{31}$$

$$T_{p2}(s) = \frac{f_2}{f_0}\left(e^{f_0 s} - 1\right) \tag{32}$$

Notice that f_0 is negative, and therefore is the rate constant that controls how fast the system comes to equilibrium over a distance s.

T_{LS}, a linear function of s, can be written:

$$T_{LS} = ms + T_{LS}^0 \tag{33}$$

which implies that m is the constant rate of change of T_{LS} over a corresponding change in position along the flow path s, and T_{LS}^0 is the temperature at land surface where groundwater flows into the domain:

$$T_{LS}^0 \equiv T_{LS}(s=0) \tag{34}$$

Under this condition, $T_{p3}(x)$ is:

$$T_{p3}(s) = \left(T_{LS}^0 + \frac{m}{f_0}\right)\left(1 - e^{f_0 s}\right) + ms \tag{35}$$

Giving the final form of the solution:

$$T(s) = \left[T_{LS}^0 + \frac{m}{f_0} + ms + \Delta T_{geothermal} + \Delta T_{viscous}\right] + \left[T_0 - T_{LS}^0 - \frac{m}{f_0} - \Delta T_{geothermal} - \Delta T_{viscous}\right] e^{f_0 s} \tag{36}$$

where f_0 is the rate constant defined by equation (21), and:

$$\Delta T_{geothermal} \equiv \frac{q_H^{base}}{\left(\frac{\sigma_{vz}}{(z_{LS} - z_{WT})}\right)} \tag{37}$$

$$\Delta T_{viscous} \equiv \frac{-\frac{Q\rho_w}{W} g \frac{dh}{ds}}{\left(\frac{\sigma_{vz}}{(z_{LS} - z_{WT})}\right)} \tag{38}$$

$\Delta T_{geothermal}$ is the change in temperature across the vadose zone required to conduct the heat flow entering the aquifer at the base (q_H^{base}), thus $\Delta T_{geothermal} > 0$ for geothermal heat flow into the aquifer. $\Delta T_{viscous}$ is the change in temperature across the vadose zone required to conduct the viscous heat generated. Note that $\frac{dh}{ds}$ is negative (i.e., decreasing head along flowpath), giving $\Delta T_{viscous} > 0$.

The simpler case of uniform T_{LS} allows an intuitive interpretation of the solution and a straightforward dimensionless analysis (below). The slope dependent terms disappear, leaving:

$$T(s) = \left[T_{LS}^0 + \Delta T_{geothermal} + \Delta T_{viscous}\right] + \left[T_0 - T_{LS}^0 - \Delta T_{geothermal} - \Delta T_{viscous}\right] e^{f_0 s} \tag{39}$$

Asymptotically, as flow proceeds along the flow path, the temperature of the aquifer must go to the temperature that balances conductive heat flow through the vadose zone with all heat added to the aquifer. This temperature is the land surface temperature plus the change in temperature required to transmit the heat through the vadose zone from the various sources:

$$T(s \to +\infty) = T_{LS}^0 + \Delta T_{geothermal} + \Delta T_{viscous} \equiv T_{+\infty} \tag{40}$$

For short distances, the temperature is dominated by the temperature of the groundwater entering the domain:

$$T(s \to +0) = T_0 \tag{41}$$

The temperature solution for the uniform land surface temperature case (equation (39)) can be written simply as:

$$T(s) = T_{+\infty} + (T_0 - T_{+\infty}) e^{f_0 s} \tag{42}$$

where $(T_0 - T_{+\infty})$ is the initial thermal perturbation relative to $T_{+\infty}$ that decays over distance.

4. Applicability of the Steady State Solution

A steady state heat and groundwater flow model might reasonably be applied to a geologic system with negligible anthropogenic influence (for example, prior to irrigated agriculture) if both of the following apply: (1) the characteristic timescale for heat conduction through the vadose zone is shorter than the time since the last significant shift in average annual land surface temperature, and (2) the changes in the basal geothermal heat flux are small on the timescale of the vadose zone heat transfer. These conditions correspond to the case where the geothermal heat flux into the aquifer is changing so slowly, compared to the equilibration time of the aquifer and vadose zone, that the geothermal heat flux can be assumed to be uniform, allowing application of a steady state solution to the system.

For groundwater systems, the time that it takes for the vadose zone to reequilibrate to new boundary conditions is generally shortened by the advection of heat by groundwater, so a conservative estimate of time of equilibration can be made by only considering heat conduction from the land surface. The characteristic timescale of conduction response ($\hat{t}$) for the vadose zone is independent of the magnitude of the temperature shift [*Deming*, 1993]:

$$\hat{t} = \frac{(z_{LS} - z_{WT})^2}{4\alpha} \tag{43}$$

with

$$\alpha = \frac{\sigma_{vz}}{\rho_s(1-\varphi)c_s + \rho_f \varphi c_f} \tag{44}$$

where the density (ρ_f) and specific heat capacity (c_f) are those of the fluid, which is air or an air-water mixture in the vadose zone. This timescale applies whether the boundary conditions change at the land surface or within the aquifer as heat is advected.

Once the vadose zone reequilibrates to a change in thermal conditions, there is a longer transient response that results from changing the temperature boundary condition on the deep geothermal system. Assuming a step change in temperature (ΔT) at the base of the aquifer, the analytic solution for the change in heat flux entering a half-space (Δq_H) is [*Turcotte and Schubert*, 2002, equation (4–116)]:

$$\Delta q_H = -\frac{\sigma_{deep}\Delta T}{\sqrt{\pi \alpha_{deep} t}} \tag{45}$$

where the subscript "deep" indicates the thermal conductivity and other properties used in the computation of α (equation (44)) and corresponds to conditions below the aquifer. While the characteristic timescale of the vadose zone is independent of the magnitude of the temperature change, the effect on the basal geothermal heat flux is not. To evaluate the effect of a temperature shift on the measured basal geothermal heat flow, both the time since a shift in average annual temperature and the magnitude of the change need to be estimated.

To account for climate variability, the principal of superposition can be used to estimate perturbations to the modern heat flux using equation (45), under the assumption that climate shifts may reasonably be approximated by step changes in temperature [*Birch*, 1948]. The influence of older climates decays at a rate of $1/\sqrt{t}$, and equation (45) can be used to show that a 10°C change in climate 1 million years ago will result in a 1–2 mW/m^2 perturbation of modern geothermal heat flow into the base of the aquifer. Therefore, assuming that 1–2 mW/m^2 is a negligible amount of heat compared to the measured geothermal heat flux, it is adequate to only consider temperature perturbations from the past million years.

Historical estimates of climate are uncertain, but *Birch* postulated six temperature histories for the past 1 million years that are generally consistent with the range of published values [*Birch*, 1948, Figure 1 and Table 4]. The climate scenarios of *Birch* are reproduced in Table 1 for use when evaluating whether or not current basal geothermal heat flow is essentially constant on the timescale of the vadose zone (estimated using equation (43)).

On the timescale of ~15 ka, a 6–7°C shift in temperature (Table 1) will result in a nonnegligible perturbation to the geothermal heat flow entering the aquifer. However, it can be demonstrated that the measured basal geothermal heat flow is essentially constant on the timescale of the vadose zone by using the derivative of (45) to estimate the rate of change of basal heat flux:

$$\frac{d(\Delta q_H)}{dt} = \frac{\sigma_{deep}\Delta T}{2\sqrt{\pi \alpha_{deep}}} t^{-3/2} \tag{46}$$

5. Development of More Complicated Models: Sequential Implementation of the Analytic Solution

For systems that can be reasonably approximated by segments that are described by piecewise-linear or piecewise-constant model input, the analytic solution can be implemented sequentially, with the output of the preceding segment becoming the input for the following segment. We developed a Python script to implement this scheme, and that script is provided in Supporting Information S2.

Model input is described in detail in Supporting Information S2, but the implementation is conceptually simple: the domain is divided into as many 1-D model segments as necessary such that the analytic solution can be applied to each segment (i.e., for each segment temperature and head vary linearly, flow is uniform, and all other parameters are uniform). Each of the inputs are defined by a separate comma-separated text file, and the Python script uses all input files to divide the domain into the number of segments required to

Table 1. The Climatic Hypotheses of *Birch* [1948] and the Resulting Effects on the Geothermal Heat Flux Into the Base of the Eastern Snake River Plain Aquifer[a]

Birch [1948] Scenario	Time of Temperature Shift (×1000 Years)														Long-Term Average (°C)	Modern Heat Flux Perturbation (mW/m^2)	Percentage of Heat Flux	Rate of Change of Heat Flux (mW/m^2/yr)	Rate of Change of Heat Flux (% in 1500 years)
	5	10	20	30	40	60	80	100	200	300	600	700	900	1000					
1A	0	2	−5	−10	−10	−10	−10	−10	−10	−10	−10	−10	−10	−10	−9.84	−19.1524	−17.4%	0.00039	0.5%
1B	0	2	−5	−10	0	−10	0	−10	2	−10	2	−10	2	−10	−2.34	−9.2091	−8.4%	0.00024	0.0%
1C	0	2	−5	−10	0	−10	0	−10	0	−10	0	−10	0	−10	−3.54	−10.3059	−9.4%	0.00024	0.0%
1D	0	2	−5	−10	−5	−10	−5	−10	0	−10	0	−10	0	−10	−3.69	−11.9873	−10.9%	0.00030	0.0%
2A	0	2	−5	−5	−5	−5	−5	−5	−5	−5	−5	−5	−5	−5	−4.94	−10.3731	−9.4%	0.00017	0.0%
2B	0	2	−5	−5	0	−5	0	−5	1	−5	1	−5	1	−5	−1.19	−5.4015	−4.9%	0.00009	0.5%

[a]*Birch* [1948] showed temperature deviation (°C) relative to the present average annual temperature for six different climate scenarios compiled from the literature. When computing perturbations to the geothermal heat flux, temperature perturbations were relative to the time-weighted average over the past 1 million years (Long-Term Average). Assuming a conservative value of thermal conductivity (2.4 W/m/°C maximizes the perturbation), the Modern Heat Flux Perturbation is computed. Assuming 110 mW/m^2 of geothermal heat flux [*Brott et al*., 1981; *Blackwell and Steele*, 1992], the Percentage of Heat Flux is shown to be nonnegligible, but the Rate of Change of Heat Flux is currently very small, indicating geothermal heat flux into the aquifer is essentially constant on the timescale of the vadose zone.

apply the analytic solution to each segment. Piece-wise linear input, hydraulic head (h), and land surface temperature (T_{LS}), are defined by a list of distances along the flow path and the corresponding values of head and temperature. Piece-wise constant input—geothermal heat flow into the aquifer (q_H^{base}), depth to water ($z_{LS}-z_{WT}$), and vadose zone thermal conductivity (σ_{vz})—are also defined by the distance at which the constant value of the parameter first applies and the corresponding value. Recharge and spring discharge are simulated as points. For recharge, the distance, recharge rate, aquifer width (W), and recharge temperature must be supplied. The flow rate entering each segment (Q) is the sum of the flow leaving the previous segment, minus spring discharge, plus additional recharge. The temperature entering each segment (T_0) is a flow weighted temperature, assuming instantaneous mixing between recharge and groundwater leaving the previous segment. If both springs and recharge are simulated at the same distance (s), computation of the new T_0 assumes that the spring temperature is the same as that of water leaving the previous segment (i.e., discharge is removed first, followed by simulation of additional recharge).

6. Example: Eastern Snake River Plain Regional Aquifer System

The Eastern Snake River Plain (ESRP) aquifer is a productive volcanic aquifer flowing generally from east to west, from near the Yellowstone Plateau to near Thousand Springs, Idaho, where much of the groundwater flow exits the system and the remaining groundwater continues to flow along the Snake River Plain [*Brott et al*., 1976, 1981; *Idaho Department of Water Resources*, 2013]. While the ESRP aquifer is locally variably confined along its length, the highly heterogeneous stratigraphy and structure generally results in unconfined conditions, well-connected to shallower geologic units. Approximately 43% of natural (i.e., not including irrigation) groundwater recharge occurs as subsurface inflow (underflow) from the surrounding uplands, 27% by infiltration from streams exiting the uplands, and the remainder from direct infiltration of precipitation [*Idaho Department of Water Resources*, 2013, Figure 55]. Along the length of the ESRP, the aquifer is commonly several hundreds of meters thick, with groundwater flow rates sufficiently large to result in very low thermal gradients (i.e., almost isothermal) within the aquifer over much of its extent, <1 to $\sim$4°C/km compared to $>$60°C/km below the aquifer [*McLing et al*., 2016]. Despite the relatively cool temperatures and low thermal gradients within the aquifer, thermal profiles for the few deep geothermal boreholes that penetrate below the aquifer indicate high geothermal heat flow ($\sim$110 mW/m^2) [*Blackwell and Steele*, 1992] compared to the global average for Tertiary tectonic provinces (70–80 mW/m^2) [*Pollack et al*., 1993].

A recent groundwater temperature map of the ESRP (Figure 2) shows a general heating trend as both geothermal and viscously generated heat accumulate along the groundwater flow path from the Yellowstone Plateau toward Thousand Springs. Cool thermal plumes associated with major tributary valleys are evident where relatively cold recharge is contributed by both subsurface flow (underflow) and infiltration from leaky streams that cross permeable ESRP geologic units near valley mouths. The rate of temperature increase with distance is much slower after a travel distance of $\sim$175 km.

Approximately 300 km of the ESRP, from near the base of the Yellowstone Plateau to the vicinity of Thousand Springs, was simulated using the piecewise analytic solution. Groundwater flow input parameters (Figure 3) were taken from the current version of the groundwater flow simulation model prepared by the

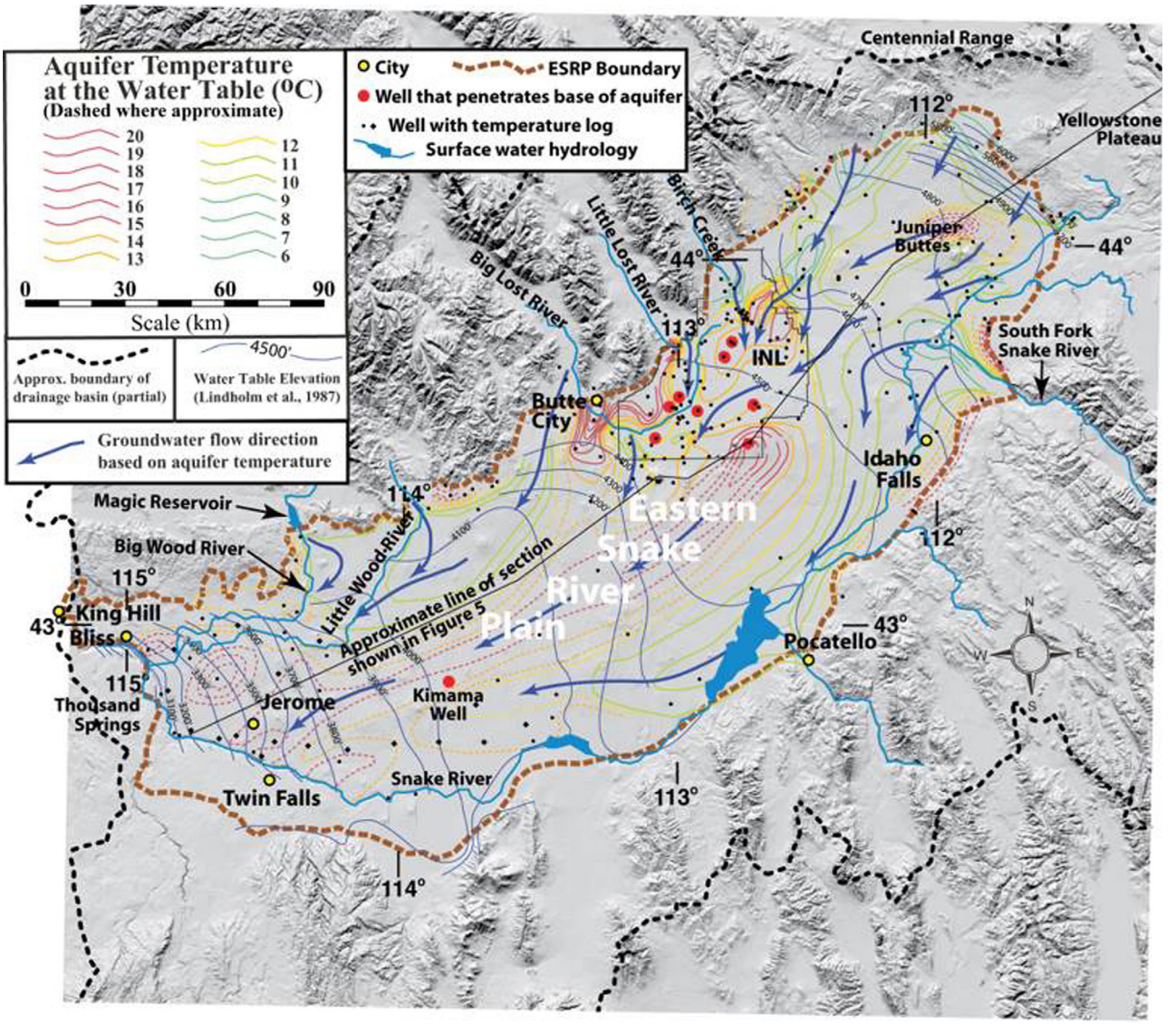

Figure 2. Map of water-table temperature for the Eastern Snake River Plain [*McLing et al*., 2016]. Groundwater flows from the Yellowstone Plateau toward Thousand Springs, with cool recharge entering as subsurface inflow, stream seepage in the vicinity of large tributary valleys, and distributed recharge from precipitation. This map provides a basis for estimating the temperature of subsurface recharge in the 1-D analytic model. The 1-D model output represents conditions along the groundwater flow path down the center of the plain, because temperatures near its margins are influenced by local groundwater mixing.

Idaho Department of Water Resources [*Idaho Department of Water Resources*, 2013]. Groundwater flow parameters are depth to water (Figure 4), head profile along the aquifer centerline, and tributary groundwater recharge rates and locations along the aquifer length. The recharge rate from precipitation (~30% of total recharge) was also taken from the IDWR model, but precipitation recharge was simply divided into equal increments and allocated pointwise every 25 km along the 300 km length. Subsurface recharge temperatures were estimated from Figure 2. Land surface temperatures were estimated from *Brott et al*. [1981, Figure 4], and the precipitation and river seepage were assumed to be at land-surface temperature. Basal heat flow was estimated as 110 mW/m^2 [*Brott et al*., 1981; *Blackwell and Steele*, 1992]. Thermal conductivity of the vadose zone was set to 1.5 W/m/°K, the median and mean value of thermal conductivity for 166 central ESRP values tabulated by *Brott et al*. [1981, Table 1b].

The steady state heat and groundwater flow model can be applied to the ESRP for the period prior to widespread anthropogenic alteration of the groundwater system (e.g., pumping and irrigation) because the vadose zone has had sufficient time to reequilibrate following the last ice age and the basal geothermal

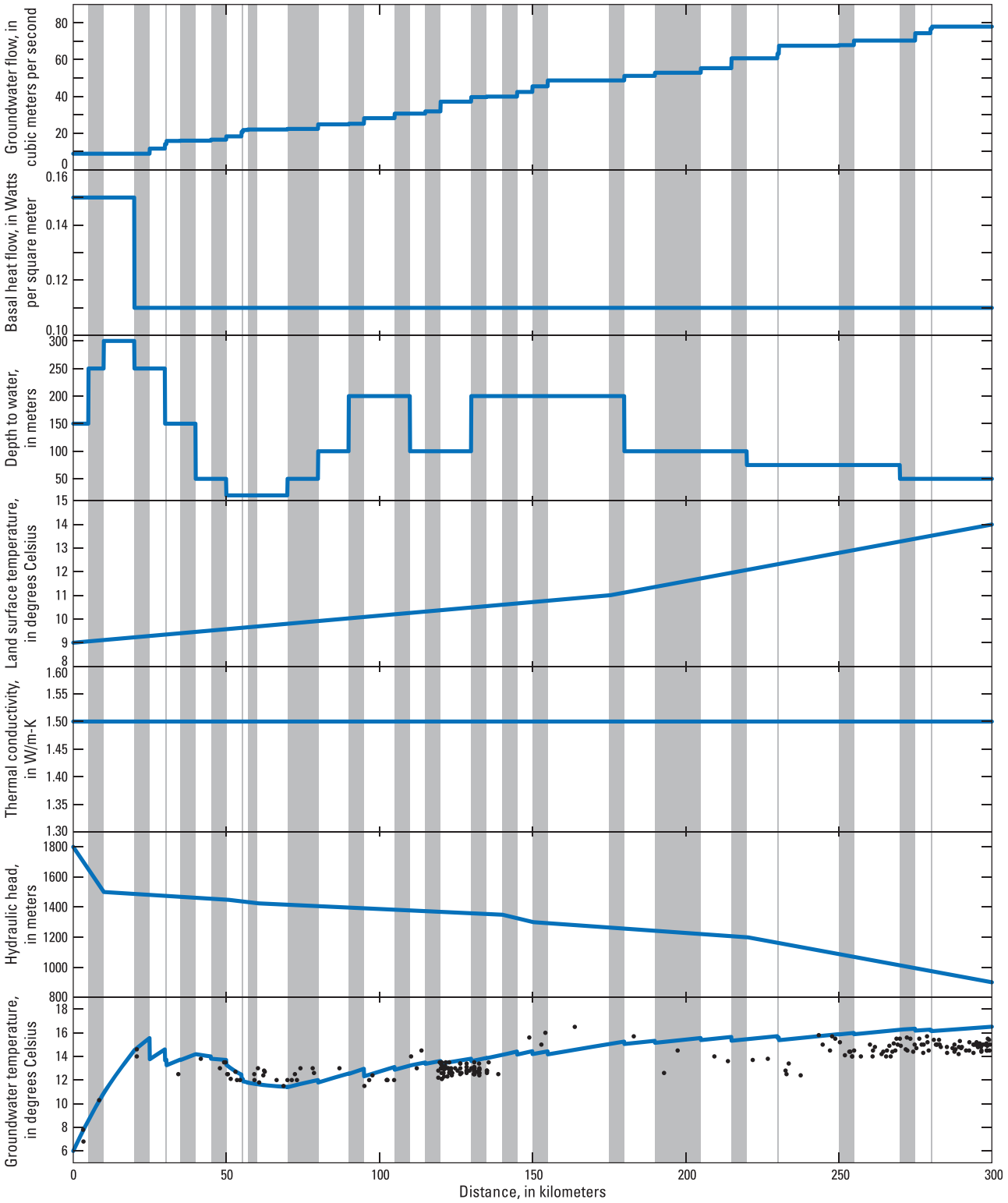

Figure 3. Input variables (all plots except the bottom) and simulated (line) and measured (points) temperature (bottom) for the Eastern Snake River Plain Aquifer. Gray-tone bars denote segment boundaries used for piecewise solution. Step changes in the groundwater temperature plot are the result of assuming instantaneous mixing between groundwater and recharge.

heat flow can be assumed to be uniform (Table 1). Using a typical ESRP vadose zone thickness (near the axis of the aquifer) of 150 m (Figures 3 and 4), the characteristic timescale is <1500 years assuming: $\sigma_{vz} = 1.5$ W/m/°C, $\rho_s \sim 3000$ kg/m^3, $c_s \sim 840$ J/kg/°C, $\rho_w \sim 1000$ kg/m^3, $c_w \sim 4{,}184$ J/kg/°C, $\rho_{air} \sim 1.2$ kg/m^3,

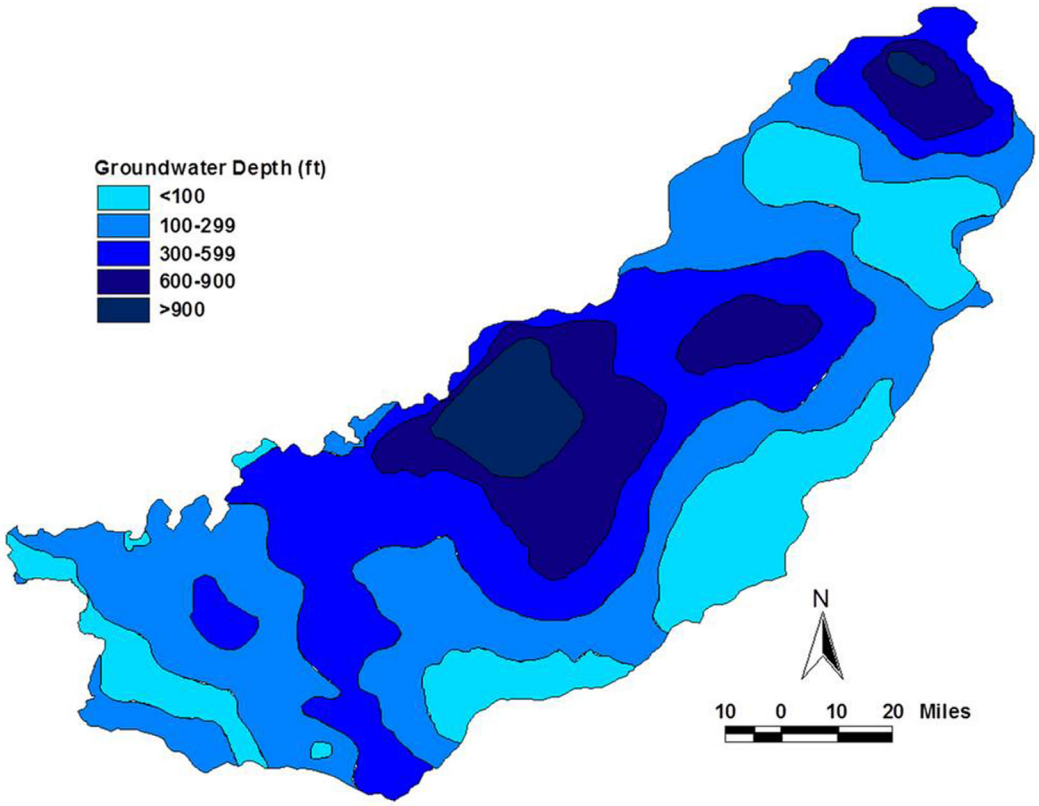

Figure 4. Example of data used to develop input for the Eastern Snake River Plain model. The depth to groundwater shown in Figure 4 was estimated from this depth-to-groundwater map for 1980 [*Idaho Department of Water Resources*, 2013, Figure 32]. Groundwater flow is from northeast to southwest, so distance is measured from the northeast edge of this map, which generally coincides with the base of the Yellowstone Plateau. Similar maps, figures, or published values were used to construct all model input (sources of each type of information are cited in the text).

and c_{air} ~1000 J/kg/°C, and φ ranging from 2.5% to 25%. Here tildes (~) are used to acknowledge that several parameters are functions of thermodynamic state variables (for example, pressure and temperature), but for the ESRP example, we assume that the variation in the parameters is small.

Recent temperature-history estimates by *Laabs et al*. [2006], namely 6–7°C increase in temperature since the last ice age (~15 ka) for nearby mountains in Utah, agree well with the estimates of *Birch* (Table 1), indicating that the *Birch* [1948] scenarios represent a reasonable range of probable thermal effects on the deep geothermal system. Assuming similar thermal properties for the deep geothermal system, except for bulk thermal conductivity (assumed to be $\sigma_{deep} = 2.4$ W/m/°C), and assuming a basal heat flow of 110 mW/m^2 and the temperature histories shown in Table 1, basal geothermal heat flux is suppressed by ~5–17% compared to the long-term steady state value. Scenario 1A (constant cooler temperatures for most of Earth's past 1 Ma) is deemed unlikely, but allows conservative estimation of the maximum possible effect. Selection of $\sigma_{deep} = 2.4$ W/m/°C is also conservative, with lesser effects for lower σ_{deep}. Evaluation of the typical expected range of σ_{deep} of 1.6–2.4 W/m/°C, and the more likely climate scenarios, indicates that geothermal heat flow at the base of the aquifer may be suppressed by 5–10%. However, for all climate scenarios, basal heat flux will change by <0.5% over the 1500 year characteristic timescale of the vadose zone (Table 1), indicating that the basal geothermal heat flow may be held constant in our simulations, and that a steady state model may be used, provided that measured basal heat flow is used as the lower boundary condition.

7. Dimensionless Numbers

The local Peclet Number (Pe_s; the ratio of advective heat transport to conductive heat transfer) describes the distance over which a thermal signal (for example, cool recharge) influences temperatures further along the groundwater flow path, and is given by:

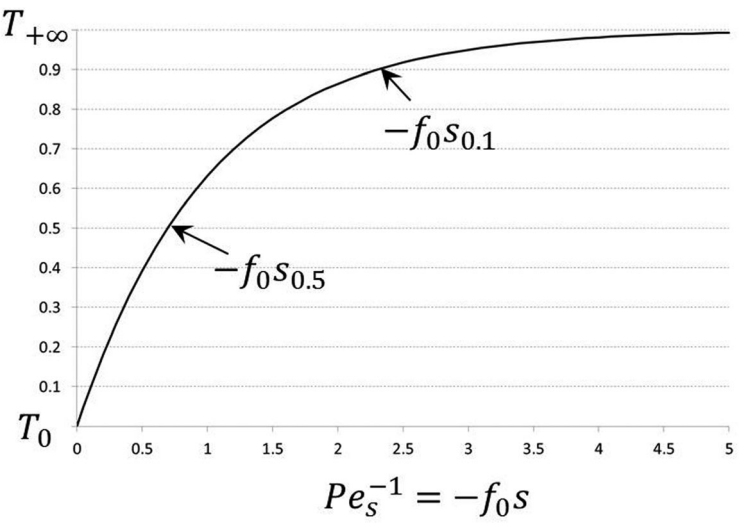

Figure 5. Plot of aquifer temperature versus dimensionless distance defined in terms of the Peclet Number. *Y* axis units are fraction of the range from the initial temperature ($\boldsymbol{T}_0$) to the asymptotic limit ($\boldsymbol{T}_{+\infty}$). Annotated points refer to the distance at which the corresponding fraction of the initial perturbation remains (see equation (48)).

$$Pe_s = -\frac{1}{f_0 s} = -\frac{Q\rho_w c_w (z_{LS} - z_{WT})}{sW\sigma_{vz}} \tag{47}$$

(see equation (21) for definition of f_0). Plotting temperature (equation (42)) against dimensionless distance ($-f_0 s$) indicates that distances with Peclet Number $\lesssim 1/3$ ($Pe_s^{-1} \gtrsim 3$) are not strongly affected by any thermal perturbations (Figure 5).

A possibly more useful dimensionless number, hereafter called the Advective Perturbation Number (AP_s), is:

$$AP_s = e^{f_0 s} = e^{-Pe_s^{-1}} \tag{48}$$

which is still well-defined for functions where f_0 is not constant:

$$AP_s = e^{\int f_0(s)ds} \tag{49}$$

AP_s describes the fraction of an advective perturbation remaining after a travel distance *s*. In other words, $AP_s = 0.9$ means that 90% of the advected thermal perturbation is still present at position *s*. Consequently, distances with $AP_s \ll 1$ are little influenced by any thermal perturbation. The Advective Perturbation Number can be used to identify the distance at which a fraction of the thermal perturbation remains using the relation:

$$s_{AP_s} = \frac{\ln(AP_s)}{f_0} \tag{50}$$

For example, 50% of the thermal perturbation remains at $s_{0.5}$ (Figure 5).

An alternate form of the Alternate Advective Perturbation Number (AP_s^{alt}) takes into account the possibility that the temperature of recharged water may be very close to the equilibrium temperature at distance *s* (i.e., the numerator term in brackets is very small compared with the denominator):

$$AP_s^{alt} = \frac{|T_0 - T_{LS}^0 - \frac{m}{f_0} - \Delta T_{geothermal} - \Delta T_{viscous}| e^{f_0 s}}{|T_{LS}^0 + \frac{m}{f_0} + ms + \Delta T_{geothermal} + \Delta T_{viscous}|} \ll 1 \tag{51}$$

While AP_s^{alt} is more unwieldy for computation, it provides additional criteria under which it is reasonable to neglect the exponential term when computing the aquifer temperature distribution—in particular, the exponential term may be neglected when T_0 is such that the numerator term in brackets is very small.

8. Discussion

Manga and Kirchner [2004] derived a solution equivalent to equation (36) under the simpler condition that $T_0 = T_{LS}^0$. *Manga and Kirchner* [2004] then further simplified the solution, considering the importance of viscous heating for the case where heat conduction to land surface is negligible (for example, high-flowrate headwater springs in the Cascade Range). Allowing T_0 to have a different value from T_{LS}^0 permits sequential application of the 1-D solution to complex geometries (for example, vadose zone thickness varying along the flow path) such as the Eastern Snake River Plain. The ESRP is a system where vadose heat conduction can be shown to be a major component of the heat budget along parts of the groundwater flow path, and

aquifer temperatures are less affected by viscous heating than a simple application of the *Manga and Kirchner* [2004] viscous-heat temperature correction would imply.

The simulated temperature from the 1-D model matches measured temperatures and the mapped temperature along the centerline of the Eastern Snake River Plain aquifer (Figure 2) reasonably well. Available groundwater and spring temperature measurements were downloaded from the USGS NWIS database (downloaded from http://waterdata.usgs.gov/id/nwis/qw on 24 Sept. 2015), filtered (as explained below), and plotted on the simulated temperature plot (Figure 3, bottom). All 441 measurements were downloaded from a 30 km wide swath through the center of the ESRP along the flow direction. Because these data were a complete (raw) dump, with no restriction based on purpose or location of sampling, the measurements were filtered to extract the general behavior of aquifer temperature, reducing the raw data by approximately 50% to 223 measurements. A 10 km moving window centered on each measurement was used to compute a median value, and if the measurement was within a 1.5°C window of the median, the measurement was retained. Further, if there were fewer than three measurements in the 10 km window, the measurement was also retained. The 1.5°C window was selected by iteration, such that the data most representative of the regional pattern are retained while removing local anomalies due to anthropogenic disturbance and still preserving a sense of the variability not captured by a simple 1-D model.

Two minor adjustments were made to calibrate the model. Vadose thickness is a relatively sensitive parameter over most of the domain, so minor adjustments to vadose zone thickness, consistent with Figure 4, were made to match an early (predevelopment) temperature measurement of 16.5°C at Thousand Springs [*Russell*, 1902, his p. 163). Also, the rate of rise of temperature in the first 20 km of the flow path (as measured relative to the Yellowstone Plateau) was too small, and was relatively insensitive to adjustments in vadose thickness, so basal heat flow was increased locally from 110 to 150 mW/m^2. This relatively modest increase in basal heat flow is consistent with proximity to the Yellowstone hotspot.

The general pattern of temperature is reproduced well, giving the magnitude and location of high, then low, measured temperatures along the first ∼70 km of the centerline with no additional adjustment of model input. The cooling of the aquifer starting at about 40 km distance results from thinning of the vadose zone (Figure 4) and addition of cool recharge (Figure 2). Prior to this distance, groundwater heats at a higher rate than in any other area, due to the combination of high head loss, thicker insulating vadose zone, higher basal heat flow, and the relatively small amount of water being heated. A better fit to the USGS NWIS temperature data in the distance range 50–80 km might easily be achieved with a minor adjustment of the vadose zone thickness, because sensitivity to this parameter is high where the vadose zone is very thin. However, *McLing et al*. [2016] mapped a region of temperatures at this distance ∼11°C, indicating that their more complete representation of the data (compared to our data filter) may support the simulated values.

Two regions of apparent bias between measured and simulated values (Figure 3, bottom) can be explained by sample bias. The cluster of low temperatures at a distance of ∼125 km were collected to the north of the aquifer centerline at the Idaho National Laboratory and are influenced by cool recharge from the Birch Creek and Little Lost River tributary valleys (Figure 2). The persistently lower temperatures (∼15°C) at distances >200 km are due to the influence of irrigation. Spring flow near Thousand Springs has increased by a factor of 5–6 since widespread irrigation projects began circa 1910, and the conceptual temperature profile for the ESRP (Figure 1) shows that flushing of irrigation water through the vadose zone will cool the aquifer.

For the ESRP, all components of heat production or loss (equation (15)) are variably important depending on distance along the flow path (Figure 6, top). Heat addition is generally from geothermal heating and viscous generation of heat, with geothermal heating significantly larger and viscous heating being (nearly) negligible over much of the length. Between 40 and 70 km distance warmer groundwater transports heat to a region with a thin vadose zone where heat is lost via conduction to the land surface. Unlike the examples considered by *Manga and Kirchner* [2004], heat conduction to land surface is not negligible for any appreciable length of the ESRP aquifer. Simulated vadose heat conduction is in the range 0–60 mW/m^2 across most of the length of the ESRP (Figure 6, top), agreeing well with mapped vadose zone heat flow estimates from above the aquifer [*Brott et al*., 1981, Figure 1 and Table 1b].

Simulated vadose zone heat conduction exceeds the basal heat input value of 110 mW/m^2 over the distance 40–70 km. The mapped vadose zone heat flow estimates of *Brott et al*. [1981] are sparse in the

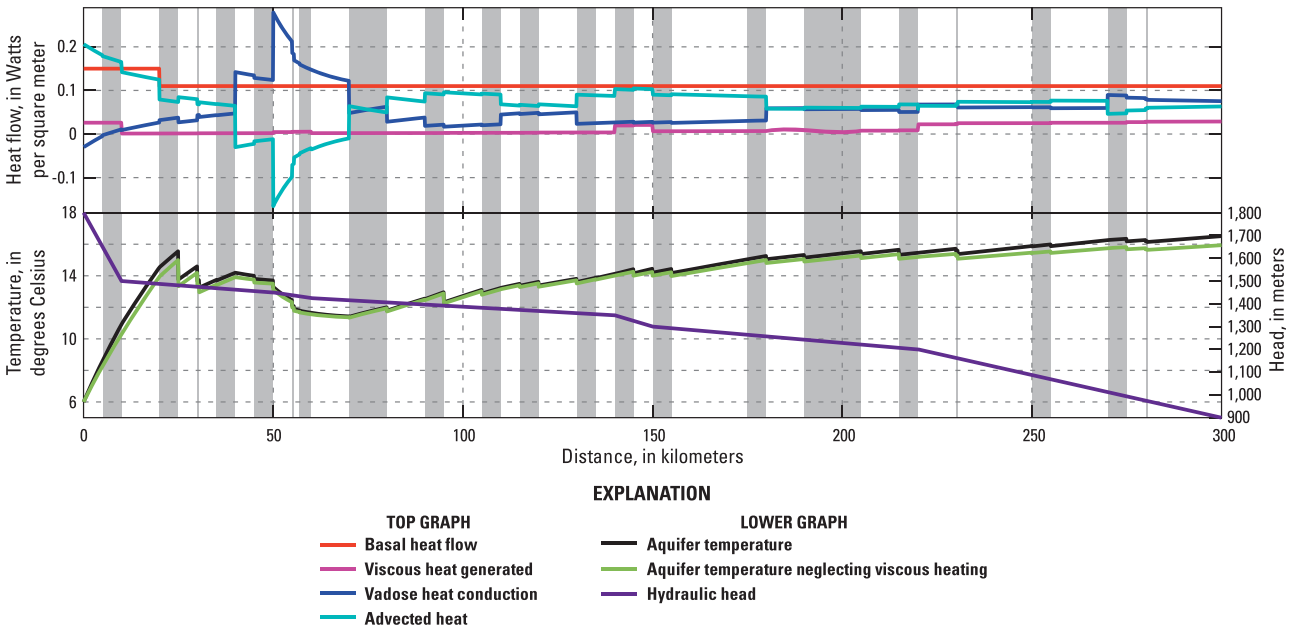

Figure 6. (top) Plot of each of the major heat-flow components (from equation (15)) along the groundwater flow path through the Eastern Snake River Plain aquifer. For ease of comparison, all heat-flow components are defined such that they are typically positive. However, total heat flow generated (basal heat flow plus viscous heat) must be balanced by the total heat flow removed (conduction to land surface plus advected heat). At ~40 km distance, the negative advected heat represents warmer groundwater flowing into a region where groundwater is cooled instead of heated. This cooling results from conduction through a relatively thin vadose zone. Elsewhere groundwater is heated by geothermal heat and viscous heat generation. (bottom) Simulated temperature for the Eastern Snake River Plain with and without viscous heating. The rate of viscous heat production is directly proportional to the rate of head loss.

vicinity of vadose thinning, potentially missing the highest vadose heat-conduction values. The extreme simulated spike of ~300 mW/m^2 is a numerical artifact associated with the step-change in vadose thickness. To better define both the simulated value and location of highest vadose zone heat flow, a refined model of vadose zone thickness should be developed. Additional data collection could then be used to verify the importance of vadose heat conduction in this part of the aquifer system.

For the Cascade Range spring systems considered by *Manga and Kirchner* [2004], viscous heating typically amounted to roughly half of the total heating along the flow path, and in fact was large enough in some instances to suggest that the geothermal heating might be negligible, in contrast to previous conclusions [*Manga*, 1998]. Because most hydrothermal heat in the Cascade Range is discharged by "slightly thermal" springs, the resulting corrections were large enough to influence heat-budget estimates for the entire volcanic arc [*Ingebritsen and Mariner*, 2010]. For the Eastern Snake River Plain, the average head gradient is smaller than the typical head gradient in the Cascades, resulting in smaller amounts of viscous heat generation compared with the other heat flow components over most of the length (Figure 6, top). Assuming a basal heat flow of 110 mW/m^2 and an aquifer width of 100 km, the total geothermal heat added along the flow path amounts to about 3300 MW; total viscous heating amounts to ~340 MW. The cumulative heat removed advected by the aquifer at 300 km distance is ~2300 MW, with the remaining heat, ~1340 MW, being removed by conduction through the vadose zone to the land surface. In this instance, the relative magnitude of viscous heating might be considered small (~10% of the total heat addition) relative to the noise and uncertainty associated with various estimates and field measurements of relevant parameters. However it can also be regarded as a systematic error that can and should be accounted for; nearly all existing hydrothermal models neglect viscous heating. The ~2300 MW of advected heat is comparable in magnitude to estimates for the U.S. part of the Cascade Range (>1000 MW) [*Ingebritsen and Mariner*, 2010] and for the Yellowstone Plateau (4000–8000 MW) [*Hurwitz and Lowenstern*, 2014].

For the simpler case where recharge temperature equals average annual land-surface temperature at the recharge location ($T_0 = T_{LS}^0$), equation (36) can be shown to be analogous to equation (3) of *Manga and Kirchner* [2004], though the parameterization is somewhat different. For the simplified geometry

and conditions (flow in an inclined aquifer with negligible heat conduction to land surface), *Manga and Kirchner* [2004] showed that viscous heat generation associated with loss of gravitational potential energy is:

$$\frac{\partial T}{\partial z} = \frac{g}{c_w} \approx 2.3^{\circ}C/\text{km} \tag{52}$$

The general derivation yielding equation (12) demonstrates that the change in temperature is more generally associated with a change in hydraulic head, regardless of geometry of the flow system. Combining equations (5) and (10) shows that the finding of *Manga and Kirchner* [2004; see also *Domenico*, 1972] holds more generally for arbitrary system geometry:

$$\frac{\partial T}{\partial h} = \frac{\frac{\partial e_m}{\partial h}}{\frac{\partial e_m}{\partial T}} = \frac{g}{c_w} \tag{53}$$

While *Manga and Kirchner* [2004] applied the $2.3^{\circ}C/\text{km}$ increase to all groundwater flow discharging at a spring, this is only appropriate where all of the groundwater flows the total distance. If groundwater accumulates over the flow path, the total viscous heat generation depends on both the groundwater flow rate and the head loss (equation (9)). For example, for the ESRP, while the head gradient is much lower for the last 70 km than for the first 10 km (Figure 6, bottom), the total viscous heat generation is a similar magnitude (Figure 6, top) due to the higher groundwater flowrate (Figure 3, top).

To understand the relative influence of viscous heating compared with geothermal heating, *Manga and Kirchner* [2004] defined a dimensionless number, Λ, which is the ratio of the geothermal warming to the viscous heat generation. This dimensionless number is related to the analytic solution presented herein as follows:

$$\Lambda = \frac{\Delta T_{geothermal}}{\Delta T_{viscous}} = \frac{-q_H^{base}}{\frac{Q}{W}\rho_w g \frac{dh}{ds}} \tag{54}$$

A sufficient condition to neglect viscous heating is $\Lambda \gg 1$ at all locations along the groundwater flow path. However, in the more general case, heat generated viscously in high-head-loss uplands may not persist to the discharge location. For example, the total simulated head loss for the ESRP is 900 m, corresponding to $\sim$2.1°C temperature increase over the total length of flow. However, simulations neglecting viscous heat generation show less than half this temperature effect at 300 km (Figure 6, bottom), mainly because of heat loss by conduction to the land surface.

The local Peclet Number ($Pe_s = (f_0 s)^{-1}$) is analogous to the β^{-1} of *Manga and Kirchner* [2004]. Writing equation (39) in terms of Pe_s and Λ gives an equation that is analogous to the equation used to generate their Figure 2a:

$$T(Pe_s) = \left[T_{LS}^0 + \left(\Delta T_{geothermal}\left(1+\Lambda^{-1}\right)\right)\right] + \left(T_0 - \left[T_{LS}^0 + \left(\Delta T_{geothermal}\left(1+\Lambda^{-1}\right)\right)\right]\right)e^{-Pe_s^{-1}} \tag{55}$$

On Figure 2a of *Manga and Kirchner* [2004], different values of Λ result in different curves, but these different curves are the result of varying the total heat addition—not just the ratio of geothermal heating to viscous heating as is implied by using Λ. In fact, if the total heating were held constant, but Λ varied, all curves on that figure would be identical. The associated assertion that for large Pe_s, viscous heating and geothermal warming dominate is incorrect; more generally, large Pe_s implies that the advective perturbation dominates.

The local Peclet Number or alternate dimensionless numbers derived above (equations (47–51)) can be used to estimate whether a thermal perturbation can be ignored when making computations. If the thermal perturbation can be ignored and an estimate of viscous heat generation can be made (equation (40)), then geothermal heat flow can be estimated from vadose-zone temperature measurements. For the ESRP, the simulation results indicate that this condition occurs only between 50 and 60 km distance along the flow path (Figure 6, top). In this area with a thin vadose zone ($\sim$20 m), Pe_s is sufficiently small to result in near equilibrium, resulting in no advective transport of heat (Figure 6, top) and resetting of the viscous heat influence on simulated temperature (Figure 6, top). Unfortunately, under practical conditions, thermal gradients at such shallow depths are also affected by factors other than the geothermal and viscous heat

production (e.g., the annual temperature wave may penetrate to 15–20 m depth). Thus, for the ESRP, reliable estimates of local variations in geothermal heat flow require measurement below the depth of vigorous groundwater flow. The good agreement between simulated (Figure 3) and mapped (Figure 2) temperatures indicates that the previous estimates of ~110 mW/m^2 for basal heat flow [*Brott et al*., 1981; *Blackwell and Steele*, 1992] are a reasonable estimate for most of the system.

9. Conclusions

The analytic solution of a simplified one-dimensional (1-D) form of the heat and groundwater flow equations derived herein includes the often-neglected viscous heat generation component of heat flow. The solution is implemented sequentially to allow simulation of moderately complex geometries; the Python code is included in Supporting Information S2. The theory and Python code are easily extendable to simulate other heat sources or sinks. Application of the 1-D solution to the Eastern Snake River Plain (ESRP) aquifer, using a priori values of input variables, shows good agreement between the simulated temperature pattern and maps of temperature prepared by *McLing et al*. [2016].

A local Peclet Number was developed, allowing the distance over which a thermal perturbation influences aquifer temperature to be estimated as a function of vadose-zone thermal conductivity, depth to groundwater, and groundwater flow rate. Even in aquifers with short equilibrium distances, variation in any of the parameters that control the Peclet Number also results in a thermal perturbation (e.g., increasing vadose thickness increases insulation between the aquifer and the land surface and results in higher temperatures), so an asymptotic approach to a constant temperature may be elusive under natural conditions.

The Eastern Snake River Plain example demonstrates that viscous heating is variably important and that heat conduction to the land surface is a primary control on the distribution of aquifer and spring temperatures. Simulation results are consistent with previous estimates of basal heat flow (110 mW/m^2) [*Blackwell and Steele*, 1992] and recently developed maps of aquifer temperature [*McLing et al*., 2016], but also suggest higher basal heat flow (~150 mW/m^2) in the easternmost part of the ESRP (the ~20 km of the ESRP nearest the Yellowstone Plateau).

Acknowledgments
The authors would like to thank the anonymous reviewers for their insightful comments and suggestions that have contributed to improve this paper. Groundwater and spring temperature measurements were downloaded from the publically accessible USGS NWIS database (downloaded from http://waterdata.usgs.gov/id/nwis/qw on 24 Sept. 2015). The Python script and all supporting input files, including data, are provided in the supporting information. Funding for this project was provided by the U.S. Department of Energy—Geothermal Technologies Program and the USGS Energy Resources Program. Funding for Michael Manga was provided by the National Science Foundation (NSF EAR-1135382). Lastly, the authors would like to thank Travis McLing and colleagues for sharing early versions of their work (for example, Figure 2), allowing us to prepare and publish this manuscript in a timely manner.

References

Anderson, M. P. (2005), Review paper/heat as a ground water tracer, *Ground Water*, *43*(6), 951–968.
Birch, F. (1948), The effects of Pleistocene climatic variations upon geothermal gradients, *Am. J. Sci.*, *246*, 729–761.
Blackwell, D. D., and J. L. Steele (1992), Decade of North American Geology (DNAG) Geothermal Map of North America: Geological Society of America, in *Decade of North American Geology Series Continent-Scale Map 006*, scale 1:5,000,000, Geol. Soc. Amer., Boulder, Colo. [Available at http://rock.geosociety.org/Store/detail.aspx?id=DNAGCSMS6.]
Brott, C. A., D. D. Blackwell, and J. C. Mitchell (1976), Heat flow study of the Snake River Plain region, Idaho: Geothermal Investigation, in *Idaho*, *Water Inf. Bull.*, *30*, Part 8, 195 pp., Idaho Dept. of Water Resour., Boise, ID.
Brott, C. A., D. D. Blackwell, and J. P. Ziagos (1981), Thermal and tectonic implications of heat flow in the Eastern Snake river plain, Idaho, *J. Geophys. Res.*, *86*(B12), 11,709–11,734.
Deming, D. (1993) Regional permeability estimates from investigations of coupled heat and groundwater flow, North Slope Alaska, *J. Geophys. Res.*, *98*(B9), 16,271–16,286.
Domenico, P. A. (1972) *Concepts and Models in Groundwater Hydrology*, 405 pp., McGraw-Hill, N. Y.
Fetter, C. W. (1994) *Applied Hydrogeology*, 3rd ed., 691 pp., Prentice Hall, Englewood Cliffs, N. J.
Forster, C., and L. Smith (1988a), Groundwater flow systems in mountainous terrain 1. Numerical modeling technique, *Water Resour. Res.*, *24*(7), 999–1010.
Forster, C., and L. Smith (1988b), Groundwater flow systems in mountainous terrain 2. Controlling factors, *Water Resour. Res.*, *24*(7), 1011–1023.
Forster, C., and L. Smith (1989), The influence of groundwater flow on thermal regimes in mountainous terrain: A Model Study, *J. Geophys. Res.*, *94*(B7), 9439–9451.
Hurwitz, S., and J. B. Lowenstern (2014), Dynamics of the Yellowstone hydrothermal system, *Rev. Geophys.*, *51*, 375–411, doi:10.1002/2014RG000452.
Idaho Department of Water Resources (2013), Enhanced Snake River plain aquifer model version 2.1, final report, 99 pp., Boise, ID. [Available at http://idwr.idaho.gov/Browse/WaterInfo/ESPAM/ESPAM_2_Final_Report/.]
Ingebritsen, S. E., and R. H. Mariner (2010), Hydrothermal heat discharge in the Cascade Range, northwestern United States, *J. Volcanol. Geotherm. Res.*, *196*, 208–218, doi:10.1016/j.volgeores.2010.07.023.
Ingebritsen, S. E., D. R. Sherrod, and R. H. Mariner (1989), Heat flow and hydrothermal circulation in the Cascade Range, north-central Oregon, *Science*, *243*,1458–1462.
Ingebritsen, S. E., W. E. Sanford, and C. E. Neuzil (2006), *Groundwater in Geologic Processes*, 2nd ed., (3rd printing with corrections). Cambridge Univ. Press, Cambridge.
Laabs, B. J. C., M. A. Plummer, and D. M. Mickelson (2006), Climate during the last glacial maximum in the Wasatch and southern Uinta Mountains inferred from glacier modeling, *Geomorphology*, *75*, 300–317.
Manga, M. (1998), Advective heat transport by low-temperature discharge in the Oregon Cascades, *Geology*, *26*, 799–802.

Manga, M. (2001), Using springs to understand groundwater flow and active geologic processes, *Annu. Rev. Earth Planet. Sci.*, *29*, 203–230.
Manga, M., and J. W. Kirchner (2004), Interpreting the temperature of water at cold springs and the importance of gravitational potential energy, *Water Resour. Res.*, *40*, W05110, doi:10.1029/2003WR002905.
McLing, T. L., R. P. Smith, R. W. Smith, D. D. Blackwell, R. C. Roback, and A. J. Sondrup (2016), Wellbore and groundwater temperature distribution Eastern Snake River Plain, Idaho; implications for groundwater flow and geothermal potential, *J. Volcanol. Geotherm. Res.*, in press.
Pollack, H. N., S. J. Hurter, and J. R. Johnson (1993), Heat flow from the Earth's interior: Analysis of the global data set, *Rev. Geophys.*, *31*(3), 267–80.
Powers, D. L. (1987), *Boundary Value Problems*, 3rd ed., 419 pp., Harcourt Brace Jovanovich, Inc., Orlando, Fla.
Russell, I. C. (1902), Geology and water resources of the Snake River Plains of Idaho, *U.S. Geol. Surv. Bull.*, *199*, 192 pp.
Saar, M. O. (2011) Review: Geothermal heat as a tracer of large-scale groundwater flow and as a means to determine permeability fields, *Hydrogeol. J.*, *19*, 31–52.
Smith, L., and D. S. Chapman (1983), On the thermal effects of groundwater flow 1. Regional systems, *J. Geophys. Res.*, *88*(B1), 593–608.
Turcotte, D. L., and G. Schubert (2002), *Geodynamics*, 2nd ed., 456 pp., Cambridge Univ. Press, Cambridge, U. K.